# Hydrate Plug Dissociation

**S. R. Davies, M. S. Selim,* and E. D. Sloan**
Center for Research on Hydrates and Other Solids, Chemical Engineering and Petroleum Refining Dept., Colorado School of Mines, 1600 Illinois St., Golden, CO 80401

**P. Bollavaram**
BP: Exploration and Production, 200 Westlake Park Blvd., Houston, TX 77079

**D. J. Peters**
Shell Global Solutions Inc., 3333 Highway 6 South, Houston, TX 77082

*DOI 10.1002/aic.11005*
*Published online October 27, 2006 in Wiley InterScience (www.interscience.wiley.com).*

*It was shown that flowline hydrate plugs dissociate radially not horizontally; this has significant implications for the remediation of a hydrate blockage, a major flow assurance problem. Over a decade of measurements has enabled models to estimate the dissociation time for hydrate plugs in flowlines, using radial heat transfer with two moving boundaries. Three different plug dissociation scenarios were modeled: single-sided depressurization, two-sided depressurization, and dissociation by radial electrical heating. The models were able to replicate the experimental observations with no fitted parameters. Structure I hydrate was found to dissociate faster than structure II; this was attributed to the different latent heats between the structures. These results indicate that hydrate dissociation in these systems is limited by heat transfer.* © 2006 American Institute of Chemical Engineers *AIChE J,* 52: 4016–4027, 2006
*Keywords: heat transfer, gas hydrates, plugs*

## Introduction

Clathrate hydrates are crystalline inclusion compounds that consist of a hydrogen bonded lattice comprised of water cages, which encapsulate small gas molecules at high-pressures and low-temperatures. Hydrates were first discovered in Birmingham, U.K. by Priestly in 1778 using a mixture of $SO_2$ and water.[2] However, it was not until 1934, after Hammerschmidt[3] discovered that hydrates were a cause of plugging of natural gas transmission lines, that significant research efforts started to focus on the conditions that lead to hydrate formation. The two most common types of hydrate structures that form from natural gas/water systems are structure I and structure II. Structure I tends to enclathrate smaller natural gas molecules, such as methane, whereas structure II tends to enclathrate larger natural gas molecules, such as propane.[1] Typically structure II hydrates form in oil and gas flowlines.

As the oil and gas industry moves into deeper water, the consequences of forming a hydrate plug are more severe. Current research is shifting from hydrate avoidance using thermodynamic inhibitors toward risk management, with kinetic inhibitors which delay the formation of hydrate, or antiagglomerants which prevent hydrate particles adhering to one another.[1]

Gas hydrates also occur naturally in oceanic sediments and permafrost regions and represent a significant energy resource.[1] The most common naturally occurring hydrate structure is structure I. Estimates of the amount of hydrate bound gas contained in these natural deposits range from $1 \times 10^{14}$ to $1 \times 10^{15}$ $m^3$ (STP).[4] Furthermore, understanding of the hydrate dissociation process, and the ability to predict the dissociation rate are important for efficient hydrate plug remediation in flowlines, and for unlocking hydrates as an energy resource. Several models have been proposed for hydrate plug remediation[5–7] including those described in this work.[8–10] This

Correspondence concerning this article should be addressed to E. D. Sloan at esloan@mines.edu.
*Deceased.

publication presents a decade of the creation, development, and experimental validation of these models in our laboratory.

The safest method of hydrate plug remediation is by two-sided depressurization below the equilibrium pressure at the seafloor temperature, for example 277 K at water depths greater than 600 m. This method avoids the formation of a pressure gradient across the plug, which could cause it to become a projectile with enough momentum to cause severe equipment damage and loss of life.[11] However, infrequently projectiles, can be created with two-sided depressurization, if multiple plugs are present with pockets of pressurized gas trapped between them.[11]

In many industrial scenarios, access to one end of the plug is restricted, and it becomes impractical to depressurize a flowline from both sides. Therefore, one-sided depressurization must be used. In this case, the hydrate plug dissociates on the downstream side, due to the lower-pressure, leading to a parabolic dissociation front. Once enough of the downstream end of the plug has melted, it is possible that the plug pressure gradient is sufficient to cause hydrate plug detachment from the pipe wall, forming a projectile, denser than the surrounding fluid. The consequences of this projectile depend on the pressure gradient, the liquid content of the flowline, and the distance to any processing equipment or radical flowline direction change.

In some deepwater field developments depressurization alone will be insufficient to bring a plug out of the hydrate stability region due to the large residual head of liquid present.[12] In these cases removal of the liquids is economically prohibitive, and heating the flowline wall to dissociate the hydrate plug may become a more economically viable alternative.

Direct electrical heating (DEH) has been used by Statoil on a number of subsea flowlines,[13,14] to keep the flowline contents above the hydrate formation temperature. However, the risk of overpressurization was considered too great to use DEH for plug remediation due to the comparatively low-flowline design pressure of 15.4 Mpa, and the high-heat flux applied.

An annular flow model has been produced[15] that shows it can be safe to apply low even levels of heat to a hydrate plug. The model demonstrates that for low-heat fluxes, gas released during dissociation is able to escape through the annulus fast enough to prevent flowline overpressurization. These findings have not yet been experimentally verified. In addition, these low-levels of heat mean that the maximum wall temperature is relatively low, and the corresponding pressure for hydrate stability is below the burst pressure of the flowline.

Two of the models described in this work, one- and two-sided depressurization,[8,9] used a boundary condition of constant pipe wall temperature. The radial electrical heating model used a constant heat-flux boundary condition. The one-sided model accounts for axial dissociation by dividing the plug into equally sized length increments, and separately tracking the pressure profile across the plug. The boundary movements are then calculated for each increment separately.

## Experimental Method

### *Hydrate formation*

Hydrate plugs were synthesized in the laboratory in a long stainless steel cylindrical cell, with five type T thermocouples ($\pm 0.5$ K accuracy) to measure the temperature at the center of the cell along the axial length (See Figure 1). The pressure at each end of the cell was monitored with pressure transducers ($\pm 5\%$ accuracy).

The hydrates were prepared from a known mass of powdered ice with a particle size range from 250–850 $\mu$m using the method described by Stern et al.[16] These ice particles provided a large surface area for contact with the gas, which increased the ability of the ice particles to absorb the exothermic heat of hydrate formation.[17] Liquid nitrogen was used to cool the cell before loading the ice, to prevent the particles from melting during the loading process. After loading, the cell was sealed, placed in a temperature controlled glycol-water bath at 271 K, and pressurized with the selected gas. The glycol water bath-temperature was then increased to 273 K to allow the ice to melt, increasing the hydrate formation rate. Occasional temperature cycling between 273 and 271 K expedited the hydrate formation. This effect was attributed to an impermeable hydrate shell forming around the water droplets, the expansion from the phase change produced fissures in the hydrate shell which permitted gas to diffuse to the free water surface.[18]

After 4–5 days the rate of pressure drop due to hydrate formation reached 1 kPa $h^{-1}$, and the hydrate formation was deemed to be complete. The hydrate conversion at this point was estimated via the moles of gas consumed, calculated using the Peng-Robinson equation of state[19] from the free-gas volume, the pressure drop, and the mass of ice. Conversions of ice to hydrate of between 98 to 100% by mass were typically achieved.

The structure I hydrate plugs were formed from pure methane (Matheson Trigas 99.99% purity). Structure II hydrates were formed from a methane-ethane mixture (65 mol% methane, 35 mol% ethane) made from pure methane (Matheson Trigas 99.99% purity) and pure ethane (Matheson Trigas 99.99% purity). The gas mixture was prepared gravimetrically (to within $\pm 1\%$). The stable hydrate structure formed with this mixture varied with pressure (See Figure 2). For example, Figure 2 shows that for a 65:35 mol% methane: ethane mixture at 273.25 K, sI will form below 9.8 Mpa, but sII will form above 9.8 MPa. The stable hydrate structure was successfully predicted using a hydrate prediction program implementing a Gibbs free-energy minimization

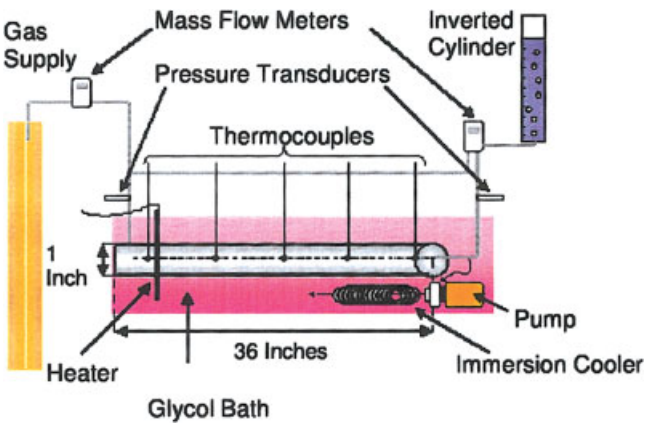


**Figure 1. Hydrate plug formation and dissociation apparatus.**

[Color figure can be viewed in the online issue, which is available at www.interscience.wiley.com.]

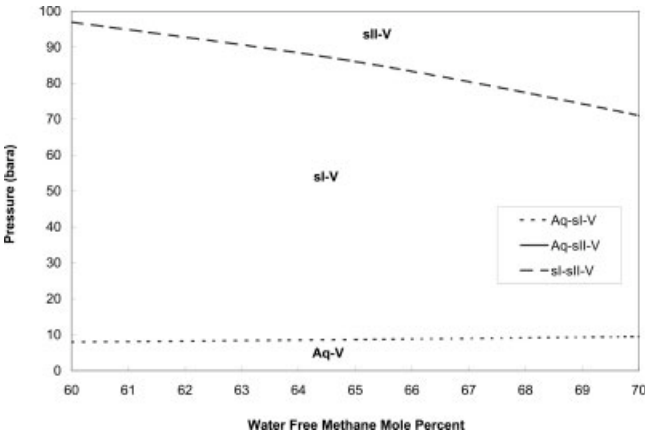


**Figure 2. Methane and ethane gas mixture at 273.25 K.**

scheme.[20] A synthetic Qatar gas mixture prepared by Scott specialty gasses (composition shown in Table 1) was used for some of the experiments.

The pressure was maintained above 9.8 MPa during hydrate formation to ensure that sII hydrate was thermodynamically stable at 273.25°C. The cell was initially pressurized to 14 Mpa, and the hydrate was allowed to form until the pressure decreased to 10 ± 0.14 MPa. The cell was then briefly depressurized to 1.4 MPa for a short period before repressurizing with the sII-forming gas mixture. This was necessary to fully replenish the original gas phase concentration. The structure of the hydrate formed was verified using Raman spectroscopy (see Figure 3). The peaks around 2,880 and 2,940 $cm^{-1}$ are assigned to the coupled C-H stretching vibration of ethane occupying the large cavities of sII. The peaks around 2,900 and 2,910 $cm^{-1}$ are assigned to the C-H stretching vibration of methane in the large and small cages of sII, respectively. The Raman peak positions compared well with published values for methane and ethane sII hydrate.[21]

### *Hydrate dissociation*

Once the hydrate plug was formed, the water-bath temperature was increased to 277 K (40 °F) to mimic typical seabed conditions. The system was allowed to equilibrate at this temperature for two hours before dissociation. The dissociation procedure was different for the two-sided depressurization, one-sided depressurization, and electrical heating experiments. In each case the rate of gas evolution from the hydrate during dissociation was measured with an inverted graduated cylinder filled with water.

**Table 1. Composition of the Synthetic Qatar Gas Mixture**

| Component | Mole % |
|---|---|
| C1 methane | 83.8 |
| C2 ethane | 7.01 |
| C3 propane | 1.6 |
| iC4 i-butane | 0.05 |
| nC4 n-butane | 0.02 |
| C5 pentanes | 0.02 |
| C6 hexanes | 0.003 |
| C7 heptanes | 0.003 |
| $N_2$ nitrogen | 4.85 |
| $CO_2$ carbon dioxide | 1.84 |

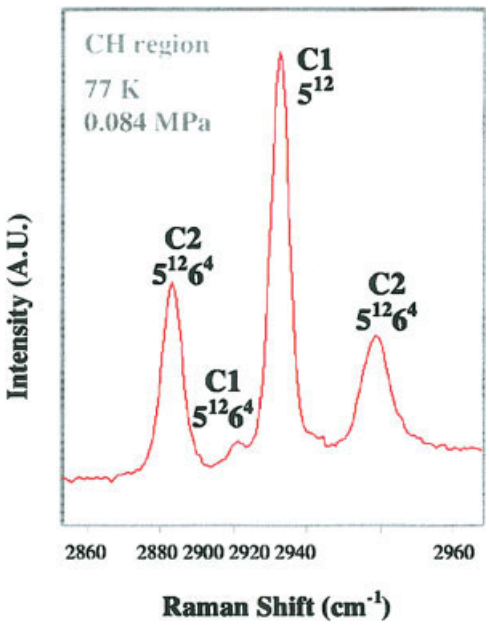


**Figure 3. Raman spectrum confirming sii hydrate was recovered from the experiment.**

[Color figure can be viewed in the online issue, which is available at www.interscience.wiley.com.]

*Two-sided Depressurization.* The hydrate plugs used to validate the two-sided depressurization model were mainly formed in a stainless steel cell 20 cm long with a 4.8 cm internal dia., which was pressure tested to 21 MPa. The hydrate plugs shown in Figure 7 were formed in a similar cell (91.4 cm in length, with a 2.54 cm internal dia.). In either case, the dissociation pressure was set using a pressure regulator or by venting the cell to the atmosphere, depending on the desired dissociation pressure.

*One-sided Depressurization.* The hydrates used to test the one-sided depressurization model were formed in a stainless steel cell (91.4 cm in length, with a 2.54 cm internal dia.). The longer cell was designed to increase the pressure difference across the hydrate during dissociation. It was also necessary to artificially reduce the permeability of the hydrates formed to ensure that the hydrate would support an axial pressure gradient during dissociation, thereby, simulating an industrially realistic dissociation by one-sided depressurization.

The permeability was reduced using a method adapted from de Boer[22] where gas is passed through the plug, causing pore filling over time, combined with the injection of a small volume of tetradecane (~100 mL freezing at 278.5 K) to reduce the pore space. The plug was then left to equilibrate at 277 K for a further two days before dissociation.

*Electrical Heating.* For the experiments to validate the electrical heating model, the cell containing the hydrates was removed from the glycol-water bath and dried. Electrical heating pads mounted on the inside of a cylindrical copper sheath to reduce the effect of hotspots, were tightly clamped to the radial surface of the cell. The cell assembly was then

wrapped in a 5 cm thick layer of ceramic insulation to reduce heat communication with the surroundings.

Prior to removal from the bath, the cell had been pressurized to either 7 or 14 MPa, depending on the dissociation pressure chosen for the experiment. This also served to increase the hydrate stability during the drying process. The equilibrium temperatures for the sI and sII hydrates are 283 K and 290 K at 7 Mpa, and 288 K and 294 K at 14 MPa, respectively.[20] The drying of the cell and mounting of the heating pads were completed within 2 min, and no measurable increase in cell temperature or pressure was noted, indicating no significant hydrate dissociation.

A variable resistor was used to set the heat input rate to the heaters. The RMS current and the potential difference of the electricity supply were monitored on multimeters and, hence, the power input could be calculated. The dissociation pressures for these experiments were controlled using needle valves to release a small volume of gas to maintain the desired pressure. The gas evolution rate was calculated from the volume of gas released, and the time for the cell pressure to recover to its original value.

## Modeling

The two-sided depressurization, one-sided depressurization and electrical heating models all assumed heat-transfer limited-radial dissociation. This assumption was later verified visually. It was assumed that the hydrate plug remained in the center of the pipe as it dissociated and was surrounded by a stationary water phase that conducted heat to the dissociating front of the hydrate plug. In this case of a plug with a dissociation temperature above the ice point (273.15 K), the problem had a single moving boundary.

In cases where the dissociation temperature of the hydrate plug was lower than the ice point, the free water produced from the dissociation process froze, forming a layer of ice around the hydrate plug. The outer radius of the ice melted to form water as heat was conducted from the pipe wall, the movement of the ice water interface was determined from the radial position at which the temperature was 273.15 K. In this case the dissociation problem had two moving boundaries. No ice phase was present in the electrical heating model as the dissociation temperature of a hydrate plug under pressure was always above the ice point.

A conceptual picture of the hydrate dissociation for each scenario is presented in Figure 4.

### *Radial dissociation model*

The limiting step in the dissociation was assumed to be the rate of heat transfer to the hydrate. This was modeled using Fourier's Law of heat transfer in cylindrical coordinates for the water and ice layers (Eq. 1)[23]

$$\frac{\partial T_W}{\partial t} = \alpha_W \left[ \frac{1}{r} \frac{\partial T_W}{\partial r} + \frac{\partial^2 T_W}{\partial^2 r} \right] \tag{1}$$

The boundary conditions used in the solution are summarized in Eqs. 2 to 9. In the depressurization models, the wall temperature was assumed to be constant (Eq. 8); in the electrical heating module the heating rate was assumed to be constant

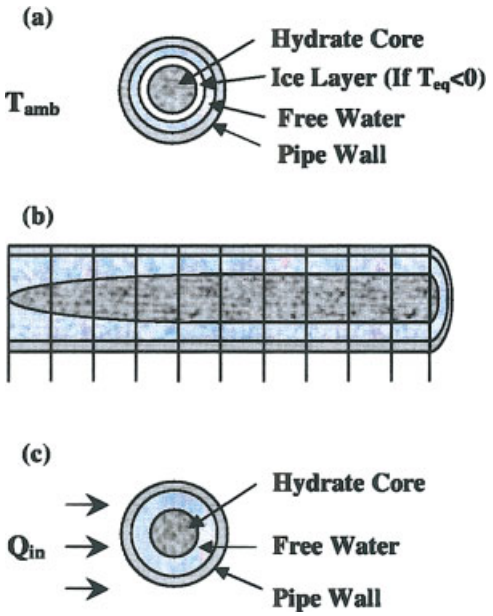


**Figure 4. Hydrate dissociation: (a) One and two-sided depressurization, (b) one-sided depressurization, and (c) electrical heating.**

[Color figure can be viewed in the online issue, which is available at www.interscience.wiley.com.]

(Eq. 9). In all of these models the temperature of the hydrate phase was assumed to be constant, with respect to the radius (that is, close to the equilibrium temperature). This assumption is valid for systems where the pressure does not accumulate significantly which would change the temperature of phase equilibrium (for example, a highly porous hydrate plug).

$$T_W = T_I; \quad r = r_I; \quad t > 0 \tag{2}$$

$$T_I = T_H; \quad r = r_H; \quad t > 0 \tag{3}$$

$$Q_I = 2\pi r_I (1-\varepsilon)\rho_I \lambda_I \frac{\partial r_I}{\partial t} + 2\pi r_I (1-\varepsilon) k_I \frac{\partial T_I}{\partial r}; \quad r = r_I; \quad t > 0 \tag{4}$$

$$Q_H = -2\pi r_H (1-\varepsilon)\rho_H \lambda_H \frac{\partial r_H}{\partial t} + \pi r_H^2 (1-\varepsilon)\rho_H C_{pH} \frac{\partial T_H}{\partial r}; \quad r = r_H; \quad t > 0 \tag{5}$$

$$2\pi r_H (1-\varepsilon) k_I \frac{\partial T_I}{\partial r} = Q_H; \quad r = r_H; \quad t > 0 \tag{6}$$

$$2\pi r_I k_W \frac{\partial T_W}{\partial r} = Q_I; \; r = r_I; \quad t > 0 \tag{7}$$

Depressurization models

$$T_W = T_0; \quad r = r_0; \quad t > 0 \tag{8}$$

Electrical heating model

$$2\pi r_0 k_W \frac{\partial T_W}{\partial r} = Q_{IN}; \quad r = r_0; \quad t > 0 \tag{9}$$

No analytical solution to the equation set was available. Therefore, the equations were solved numerically by setting up a finite difference grid and used the standard explicit scheme to calculate the water temperatures at the next time step. The time step was chosen to be small enough to prevent the solution from diverging.[24]

### *One-sided depressurization model*

The one-sided depressurization model had an additional level of complexity, since it modeled the axial pressure profile along the length of the plug which led to different radial dissociation rates along the length of the hydrate plug. The dissociation rate of a hydrate is faster the further it is outside of the phase equilibrium envelope.[1]

An initial condition of constant temperature and pressure across the plug was used. The depressurization was represented by imposing a step change in downstream pressure at $t = 0$. The plug was modeled as two separate elements: the upstream section still in contact with the pipe, and the dissociating downstream section.

The axial pressure profile in the upstream section was then modeled by assuming the downstream section was fixed, and combining Darcy's law with the ideal gas equation for molar volume. Since the timescale of gas convection through the plug was much faster than the timescale for the dissociation of the hydrate plug, the hydrate plug was at a quasi-steady state relative to the gas convection. The effects of the dissociation rate on the determination of the pressure and temperature profiles, and on the gas composition were therefore negligible

$$\frac{d}{dz}\left[-\rho\frac{\kappa}{\mu}\frac{dP}{dz}\right] = 0 \tag{10}$$

As the pressure in a length increment fell below the equilibrium pressure, the radial dissociation model was initiated, and the dissociation rate was calculated. Once the annulus spacing required for pressure communication was reached (defined as 8% of the radius for these simulations), the pressure at this axial position was assumed to be equal to the downstream pressure.

Axial-heat transfer by convection and conduction in the gas phase, and by conduction in the hydrate phase were included in the energy balance. The gas and hydrate phases were assumed to be in thermal equilibrium at each axial distance. The model was also adapted to include Joule-Thompson cooling in the energy balance. The temperature profile was solved by the upwinding difference method to overcome stability problems when the convection term became dominant

$$(\rho C_p)_f v_z\frac{dT}{dz} - \beta T v_z\frac{dP}{dz} = (\varepsilon k_f + (1-\varepsilon)k_h)\frac{d^2T}{dz^2} \tag{11}$$

The following dimensionless terms were used to solve the pressure, velocity and temperature profiles

$$\phi = \frac{(P-P_d)}{(P_u-P_d)}; \quad N = \frac{P_u}{P_d}; \; \eta = \frac{z}{L_c}; \quad \theta = \frac{T_h - T_d}{T_u - T_d}; \quad W = \frac{T-T_0}{T_D - T_0}$$

The dimensionless form of the pressure equation and associated boundary conditions are:

$$\frac{d^2}{dz^2}\left(\phi^2 + \frac{2\phi}{N-1}\right) = 0 \tag{12}$$

$$\phi = 1 \quad \eta = 0 \tag{13}$$

$$\phi = 0 \quad \eta = 1 \tag{14}$$

The analytical solution to this problem was given by Morrison[25]

$$\phi = \frac{\left\{\sqrt{N^2-(N^2-1)\eta}\right\} - 1}{N-1} \tag{15}$$

The fluid velocity was calculated from Darcy's law (Eq. 16) using the differentiated form of Eq. 15 shown in Eq. 17. The equation for the resulting velocity profile is shown in Eq. 18

$$v_z = -\frac{\kappa}{\mu}\frac{dP}{dz} \tag{16}$$

$$\frac{d\phi}{d\eta} = \frac{-(N+1)}{2\sqrt{N^2-(N^2-1)\eta}} \tag{17}$$

$$v_z = \frac{\kappa P_d}{2\mu L_c}\frac{(N^2-1)}{\sqrt{N^2-(N^2-1)\eta}} \tag{18}$$

The axial temperature distribution shown in Eq. 19 was found by rewriting Eq. 11 in terms of the dimensionless variables

$$\frac{d^2\theta}{d\eta^2} - F_t f(\eta)\frac{d\theta}{d\eta} - F_t\,\beta\,P_d\,g(\eta)\theta = F_t\,\beta\,P_d R_T\,g(\eta) \tag{19}$$

Where:

$$F_t = \frac{\kappa\,P_d}{\mu\,\alpha_m} \tag{20}$$

$$f(\eta) = \frac{N^2-1}{\sqrt{N^2-(N^2-1)\eta}} \tag{21}$$

$$g(\eta) = \frac{(N^2-1)^2}{N^2-(N^2-1)\eta} = [f(\eta)]^2 \tag{22}$$

$$R_t = \frac{T_d}{T_u - T_d} \tag{23}$$

The appropriate boundary conditions are shown below.

$$\theta = 1 \quad \eta = 0 \tag{24}$$

$$\theta = 0 \quad \eta = 1 \tag{25}$$

The temperature profile was solved numerically; two different solution schemes were needed for a stable solution, owing to the dominance of convection over diffusion:[26] classical center-difference scheme, and upwind-differencing scheme.[27]

The upwinding-difference scheme used a backward difference for the first spatial derivative, and a centered difference for the second spatial derivative

$$\frac{d\theta}{d\eta} = \frac{W_i - W_{i-1}}{\Delta x} \tag{26}$$

$$\frac{d^2\theta}{d\eta^2} = \frac{W_{i+1} - 2W_i + W_{i-1}}{\Delta x^2} \tag{27}$$

Substitution of the derivative approximations into Eq. 19 resulted in Eq. 28.

$$\left(\frac{A1}{\Delta x} - \frac{1}{\Delta x^2}\right) W_{i-1} - \left(\frac{2}{\Delta x^2} + \frac{A1}{\Delta x} + A2\right) W_i + \left(\frac{1}{\Delta x^2}\right) W_{i+1} = A3 \tag{28}$$

where

$$A1 = F_t f(x_i), \quad A2 = F_t \beta P_d g(x_i), \quad A3 = A2R_t \tag{29}$$

The solution to the upwinding difference scheme was obtained by setting up a tridiagonal matrix and solving for the dimensionless temperatures: the Thomas algorithm.[28]

The numerical solution was verified by comparison with an analytical solution to a simplified form of the temperature equation in which the work done by pressure was neglected. The resulting equation is shown below in terms of the dimensionless variables

$$\frac{d^2\theta}{d\eta^2} = F_t f(\eta) \frac{d\theta}{d\eta} \tag{30}$$

The analytical solution to this problem is shown in Eq. 31

$$\theta = \frac{A(a, \eta = 1, F_t') - A(a, \eta, F_t')}{A(a, \eta = 1, F_t') - A(a, \eta = 0, F_t')} \tag{31}$$

where

$$A(a, \eta, F_t') = e^{-\frac{2F_t'}{a}\sqrt{1-a\eta}} \left(\sqrt{1 - a\eta} + \frac{a}{2F_t'}\right) \tag{32}$$

$$a = \frac{(N^2 - 1)}{N^2}, \quad F_t' = F_t \left(\frac{N^2 - 1}{N}\right) \tag{33}$$

The numerical solution was compared to the analytical solution in Figure 5 for the case where the dimensionless pressure drop $N = 2.2$, and permeability $\kappa = 0.01$ mD. It can be seen that for 25 steps the numerical solution is a good approximation to the analytical solution.

### *External heat-transfer resistance model*

The additional heat-transfer resistance from external insulation or surrounding sediment for a buried flowline was modeled using a Biot number. The Biot number expresses the dimensionless ratio of the external heat-transfer resistance to the heat-transfer resistance of the pipe wall. The Biot number was used to scale the pipe wall temperature between the temperature of the pipe contents, and the ambient conditions.

The only modification to the equation set needed to incorporate the heat-transfer resistance term was the modification of the boundary condition (Eq. 8) from constant to a transient

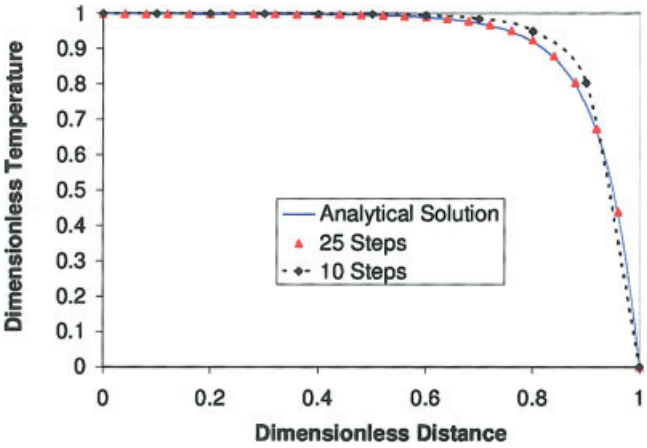


**Figure 5. Comparison of the numerical solution (points) for 10 and 25 length increments to the analytical solution (line) for $N$ = 2.2, and $\kappa$ = 0.01 mD.**

[Color figure can be viewed in the online issue, which is available at www.interscience.wiley.com.]

temperature. The instantaneous boundary condition was found from Eq. 34. An iterative method was used to arrive at the correct initial temperature at the pipe wall.

$$\frac{dY}{dR} = Bi[Y - 1]; \quad R = R_H; \quad t^* > 0 \tag{34}$$

where

$$Bi = \frac{hr_0}{k_{wall}} \tag{35}$$

## Results and Discussion

The assumption that the rate of radial dissociation would be significantly greater than the axial dissociation was verified by opening the cell, and observing the dissociation after one, two and three hours (See Figure 6). Recently computer tomography (CT) images[29] have confirmed the predominance of radial dissociation.

The models developed in this work were verified by comparing the predicted results to a series of experiments. The hydrate plug porosities used in the model were calculated for each experiment using the initial mass of ice added to the cell, and the volume of gas evolved during the experiment. The evolved gas was compared to the gas consumed during formation, which was calculated based on the pore space, and the total pressure drop using the Peng-Robinson equation of state. Mass balance closures within 5% were typical.

The model predicted the position of the dissociating front of the hydrate plug as a function of time for each experiment. This was used to calculate a corresponding gas evolution rate. The predicted gas evolution was then compared to the experimentally observed gas evolution rate.

### *Two-sided depressurization*

During the two-sided depressurization experiments, several different types of experiments were performed in order to validate the model. The latent heat of dissociation is higher

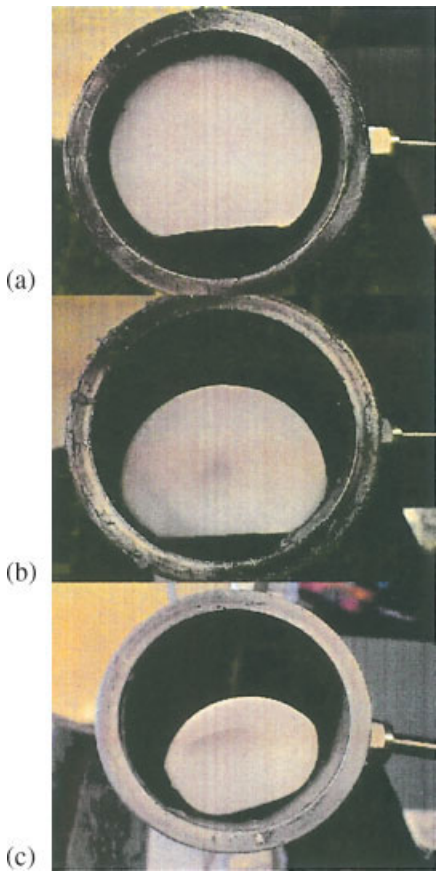


**Figure 6. Photographs of hydrate dissociation by pressure reduction after: (a) 1 h, (b) 2 h, and (c) 3 h.**

[Color figure can be viewed in the online issue, which is available at www.interscience.wiley.com.]

for sII hydrates (640.15 kJ/kg) than sI (460.24 kJ/kg),[1] hence, the model predicted that sII would dissociate more slowly; this was confirmed experimentally for the methane-ethane gas mixture. The model predicted this difference in dissociation time to a good accuracy (See Figure 7). However, some experiments using the synthetic sII forming Qatar gas mixture dissociated significantly faster than the prediction.[8] This was attributed to the rapid depletion of the sII formers during formation meaning that the sample contained predominantly sI.

The time for the ice plug to melt was defined as the time for the thermocouple readings to increase above 273.15 K. This is likely to be less than the actual time to melt the ice plug as the ice may detach from the thermocouples as the plug melts.

The total ice-hydrate plug remediation times were found to be significantly greater at elevated pressures (higher-dissociation temperatures) for the same hydrate porosities and ambient temperatures (See Table 2). This indicated that the fastest way to remediate a hydrate blockage is to depressurize the flowline as quickly and to as great an extent as possible. The additional time required to melt the resultant ice plug was offset by the faster hydrate plug dissociation time. This was attributed to a combination of the higher driving force, the latent heat released from the water freezing and the higher-thermal diffusivity of ice ($1.2 \times 10^{-6} m^2/s$) compared to water ($1.3 \times 10^{-7}$ $m^2/s$).[30] Dissociation experiments were also performed on partially converted hydrate plugs. The dissociation time was found to be substantially faster for lower hydrate conversions.[31] This effect can be attributed to the additional heat provided by the unconverted water freezing during dissociation.

The assumptions made for the radial dissociation model limit it to an order of magnitude estimate of total dissociation time. That is, the plug is assumed to remain at the center of the pipe throughout the dissociation, and the remaining volume of the flowline is filled with water. In reality buoyancy effects, and the effect of a hydrocarbon phase on the fluid thermal diffusivity will influence the heat-transfer rate. The effect of the higher-thermal diffusivity of the aqueous phase compared to the gas phase on the radial dissociation rate is clearly illustrated in Figure 6. The free-water produced from the hydrate dissociation drains to the bottom of the cell due to the density difference, leading to faster hydrate dissociation below the gas water interface.

The surrounding fluid composition and the liquid volume fraction for an industrial hydrate plug will depend on flowline geometry and plug location and can rarely be predicted. The model is particularly sensitive to plug porosity, which is rarely known in an industrial situation. Although based on a limited data set, a porosity of 0.5 seems to represent the melting of a hydrate plug reasonably well.

### *One-sided depressurization*

During the one-sided depressurization experiments, several different types of experiments were performed in order to validate the model. The permeability of the hydrate plug was artificially reduced in order for the plug to sustain an axial pressure gradient during dissociation. Despite the attempts to reduce the permeability by injecting tetradecane, it was still necessary to depressurize the plug in stages to prevent premature pressure communication. The upstream pressure was maintained above the equilibrium pressure while the downstream pressure was reduced. Experiments were performed

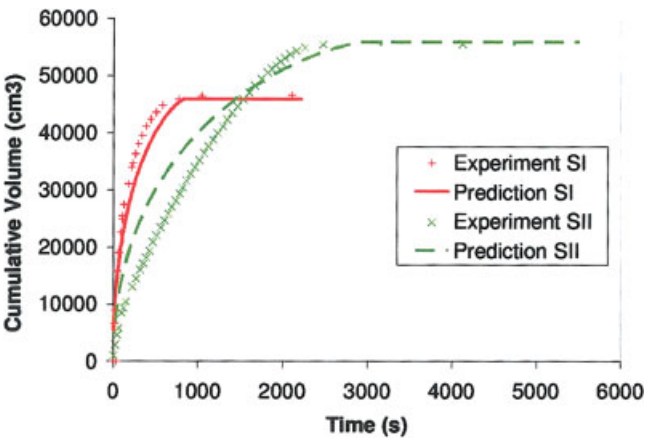


**Figure 7. Comparison of Structure I and structure II hydrate plug dissociation results with two-sided depressurization model.**

[Color figure can be viewed in the online issue, which is available at www.interscience.wiley.com.]

**Table 2. Experimental Results and Two-Sided Depressurization Model Predictions for sI Hydrate/Ice Dissociation at Various Conditions**

| Porosity | Ambient Temperature (°C) | Dissociation Temperature (°C) | Phase | Pred. (hrs) | Obs. (hrs) |
|---|---|---|---|---|---|
| 0.28 | 1 | −1 | Hyd. | 6.1 | 3 |
| | | | Ice | 7.3 | 4.5 |
| 0.28 | 3.3 | −1 | Hyd. | 7.6 | 5.8 |
| | | | Ice | 15 | >7 |
| 0.28 | 4.6 | −1 | Hyd. | 4.1 | 2.2 |
| | | | Ice | 6.0 | 4.6 |
| 0.3 | 4.6 | −0.2 | Hyd. | 6.3 | 3.3 |
| | | | Ice | 6.7 | 5.2 |
| 0.32 | 4 | −0.3 | Hyd. | 6.6 | 3.7 |
| | | | Ice | 7.3 | 5.5 |
| 0.32 | 4.1 | −0.8 | Hyd. | 4.8 | 3.2 |
| | | | Ice | 6.5 | 5.0 |
| 0.33 | 4.1 | −0.4 | Hyd. | 6.0 | 3.8 |
| | | | Ice | 6.9 | <6 |
| 0.35 | 4.1 | −1 | Hyd. | 3.9 | 4.0 |
| | | | Ice | 6.0 | 5.8 |
| 0.36 | 4.1 | −0.4 | Hyd. | 5.8 | 3.3 |
| | | | Ice | 6.6 | <5 |
| 0.37 | 4.1 | −0.8 | Hyd. | 4.4 | 4.0 |
| | | | Ice | 6.0 | 5.3 |
| 0.43 | 4.1 | −6.5 | Hyd. | 0.75 | 0.88 |
| | | | Ice | 4.0 | 5.0 |

with pressure drops of around 0.2 MPa. The bath temperature was maintained at 277.15 K for all experiments.

From the pressure transducer readings it was noted that pressure communication was established approximately half an hour into the experiment. From this point the hydrate was depressurized from both sides and was modeled accordingly. The predicted and experimentally observed gas evolution for one of the plugs is shown in Figure 8. The plug porosity was initially 0.54, but was reduced to 0.22 by adding 150 mLof hydrocarbon. The total time for the hydrate to dissociate is underpredicted by 9.1% in this case. Most of this difference occurs in the first part of the experiment before pressure communication is established (see Figure 8).

When modeling the one-sided depressurization experiments, the effect of permeability on the predicted dissociation time was found to be small due to the low pressure difference across the plug. The thermal diffusivity used in each simulation was calculated based on the hydrate/hydrocarbon volume fraction on a volume averaged basis using the arithmetic model.[32]

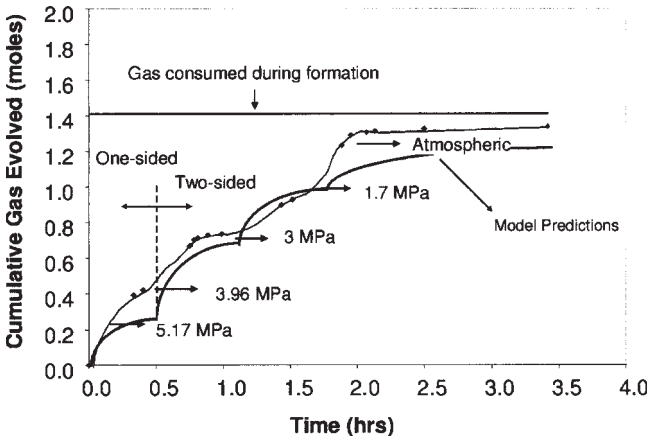


**Figure 8. Comparison of structure I hydrate plug dissociation results for staged pressure reduction with the one-sided depressurization model.**

It was attempted to compare the model to published industrial cases of hydrate plug dissociation by one-sided depressurization. Two such dissociation cases are reported for the Tommelieten field in Norway.[33] One plug took 25 days to dissociate, while the other plug dissociated after nine days. When modeling an industrial hydrate plug there is currently little knowledge of the plug porosity, permeability and plug length which makes it difficult to accurately model these field experiments.

A sensitivity analysis of the effect of permeability shows the total dissociation time deviates by less than a factor of two when permeability is varied by two-orders of magnitude. A permeability of $1 \times 10^{-11}$ m$^2$ was used for the simulations which is consistent with published values for $CCl_3F$ hydrate plugs.[34]

Porosities between 0.3 and 0.8 were investigated. An annulus spacing of 8% of the pipe diameter was chosen as an indication of when pressure communication is established, this was based on laboratory observations. The predicted dissociation time increased linearly with plug length. In most industrial applications plug length is rarely known; it is, therefore, advised that several calculations be performed for a range of realistic lengths. For our calculations the hydrate plug length was fit to the time to dissociate the hydrate. A summary of the data is shown in Table 3.

The calculated plug lengths are significantly greater than those estimated in the article of 1–20 m,[33] which were made based on the low-water cut ~2% in the flowline. The model consistently overpredicted the dissociation time for the laboratory scale experiments, but consistently underpredicted the field-test dissociation tests. The reason for the discrepancies with the laboratory data may stem from the problems encountered when trying to reduce the plug permeability by injection of a liquid hydrocarbon phase. This may have led to an inhomogeneous plug with an uneven pressure profile.

The discrepancies between the estimated plug lengths in Tommelieten tests, and the plug lengths predicted by the model are likely to be due to the lower-thermal diffusivity of the predominantly gas continuous phase in the flowline, compared to water as assumed in the model. Another explanation could be the movement of chunks of the hydrate plug during dissociation causing secondary plugs to form.

### *Electrical heating*

Eighteen experiments were conducted in total. Power inputs of 10, 20 and 30 W were investigated for both sI and sII natural gas hydrates at dissociation pressures of 7 MPa and 14 MPa.

The model predictions were found to be in good agreement with the experimental observations for both sI and sII hydrates (see Figure 9). The predicted delay times for some of the experiments, before the dissociation commencing show discrepancies with the experimental observations. Specifically, the model predicts the dissociation will start earlier than is physically observed. This difference is attributed to

**Table 3. Calculated Plug Lengths for the Tommelieten Experiments[33]**

| | |
|---|---|
| **Plug 1:** | |
| Upstream Pressure (MPa) | 8.96 |
| Downstream Pressure (MPa) | 0.68 |
| Equilibrium Pressure (MPa) | 1.38 |
| Ambient Temperature (K) | 277.15 |
| Permeability ($m^2$) | $1 \times 10^{-11}$ |
| Diameter (m) | 0.152 |
| Dissociation Time (days) | 25 |
| Porosity | Predicted Length (m) |
| 0.3 | 91 |
| 0.4 | 104 |
| 0.5 | 120 |
| 0.6 | 146 |
| 0.7 | 183 |
| 0.8 | 252 |
| **Plug 2:** | |
| Upstream Pressure (MPa) | 5.37 |
| Downstream Pressure (MPa) | 1.24 |
| Equilibrium Pressure (MPa) | 1.38 |
| Ambient Temperature (K) | 277.15 |
| Permeability ($m^2$) | $1 \times 10^{-11}$ |
| Diameter (m) | 0.152 |
| Dissociation Time (days) | 9 |
| Porosity | Predicted Length (m) |
| 0.3 | 74 |
| 0.4 | 81 |
| 0.5 | 98 |
| 0.6 | 117 |
| 0.7 | 144 |
| 0.8 | 206 |

the neglecting of heat-transfer resistance in the hydrate phase and to the contribution of the cell wall; the cell wall must be heated from the water-bath temperature (277 K), to the hydrate dissociation temperature which may be up to 289 K.

A summary of the experimental results and heat-transfer model predictions is provided in Table 4.

The sensitivity of the heating module to the presence of an oil phase during dissociation was investigated. The resulting dissociation rate was qualitatively compared to the model

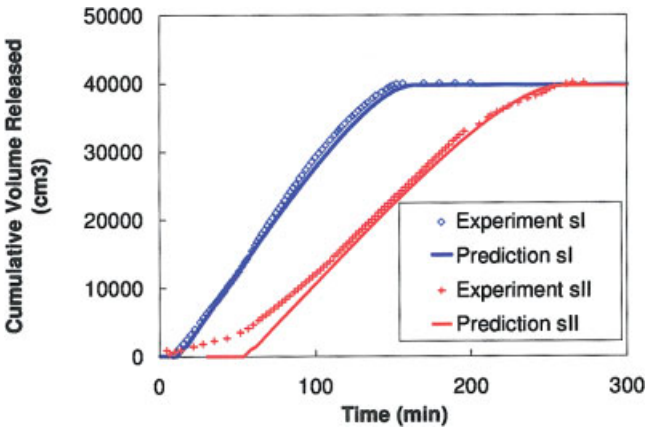


**Figure 9. Comparison of experimental results for structure I and structure II hydrate plugs with the electrical heating model (10 W, 14 MPa).**

[Color figure can be viewed in the online issue, which is available at www.interscience.wiley.com.]

**Table 4. Experimental Results and Heat Transfer Model Predictions for sI and sII Hydrate Dissociations at Various Conditions**

| Pressure | 7 MPa | | 14 MPa | |
|---|---|---|---|---|
| Time (min) | Pred. | Obs. | Pred. | Obs. |
| **Structure I** | | | | |
| 10 W | 163.7 | 156.3 | 209 | 237.9 |
| 20 W | 92.2 | 96 | 119.5 | 120.3 |
| 30 W | 80.9 | 84 | 85.4 | 91.8 |
| **Structure II** | | | | |
| 10 W | 228.7 | 265.6 | 436.3 | 362.7 |
| 20 W | 191.9 | 157.8 | 221.3 | 183 |
| 30 W | 145.1 | 125.3 | 169.2 | 179.8 |

prediction and to the dissociation rate of a hydrate under the same conditions without an oil phase present. The oil was injected into a preformed structure I hydrate plug using gas displacement.

A low-viscosity crude oil from the ExxonMobil Conroe field (as shown in Table 5) was chosen to facilitate the maximum possible filling of the hydrate pore spacing. Twenty watts of heat was applied evenly to the radial surface of the hydrate plug, and the free gas was released from the cell to maintain the pressure at 7 MPa. The rate of gas evolved from the dissociating hydrate plug was compared to that of a hydrate plug dissociated under the same conditions without an oil phase present. It can be seen from Figure 10 that the presence of the oil phase increases the dissociation time by approximately 10%. It is likely that this effect is attributable to the oil phase consuming some of the heat transferred from the pipe wall as the contents are heated. The pressure transducer readings at either end of the cell coincided throughout the experiments both with and without an oil phase, even though the dissociated gas was only released from one side of the plug, indicating good pressure communication.

An important consideration when dissociating a hydrate plug in the field is the maximum pressure accumulation that can occur during dissociation if the gas is contained by impermeable plugs at either end of the heated section. Two experiments were conducted in this work, involving dissociating structure I methane hydrate plugs in a closed system. The first experiment was performed without an oil phase

**Table 5. Composition of the Conroe Oil by Chromatograph**

| Component | Mole % |
|---|---|
| C1 methane | 0.008 |
| C2 ethane | 0.011 |
| C3 propane | 0.117 |
| iC4 i-butane | 0.126 |
| nC4 n-butane | 0.366 |
| iC5 i-pentane | 0.620 |
| nC5 n-pentane | 0.707 |
| C6 hexanes | 2.075 |
| C7 heptanes | 6.906 |
| C8 octanes | 13.546 |
| C9 nonanes | 10.423 |
| C10 decanes | 8.179 |
| C11 undecanes | 6.306 |
| C12 dodecanes | 6.100 |
| C13 tridecanes | 6.966 |
| C14 tetradecanes | 6.382 |

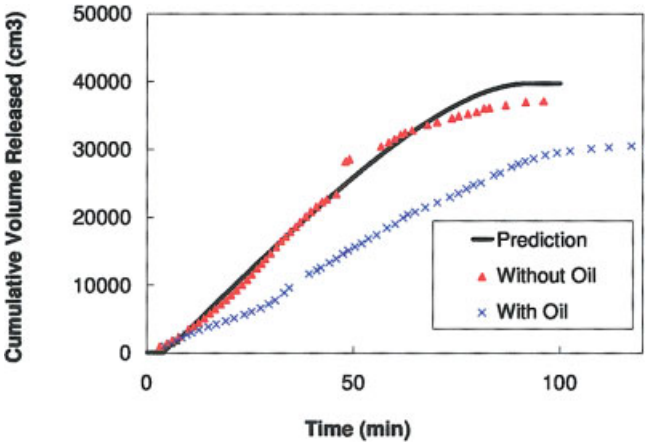


**Figure 10. Comparison of the dissociation rate of a hydrate plug with and without the presence of a liquid hydrocarbon phase.**

[Color figure can be viewed in the online issue, which is available at www.interscience.wiley.com.]

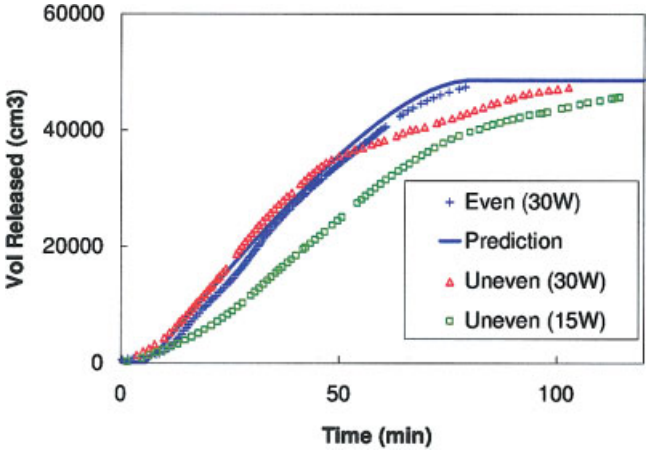


**Figure 12. Comparison of dissociation rates for uneven heating to even heating.**

[Color figure can be viewed in the online issue, which is available at www.interscience.wiley.com.]

present. This experiment served to give confidence in the theoretical calculations before the gas volume was reduced by addition of an oil phase in the second experiment.

In both experiments, the cell was initially depressurized to 3.5 MPa and then sealed. Twenty watts of heat was applied evenly to the radial surface of the hydrate plugs. The gas released by the dissociation was contained inside the cell. The gas pressure at either end of the cell was constantly monitored with pressure transducers. The results of the experiments are shown in Figure 11. The upstream and downstream pressures were coincident in the experiments.

Figure 11 clearly shows that the addition of the oil phase significantly increases the rate of pressure build up in the system. With all the pores in the hydrate plug filled with oil, the pressure needed to be manually relieved three times to prevent it exceeding the cell test pressure of 21 MPa. The manual releases of gas can be seen on the figure as a sawtooth profile between 90 and 110 min. A total of 3,000 $cm^3$ of gas was released during this venting. This corresponded to less than 10% of the total dissociated gas from the hydrate plug (41,000 $cm^3$), which was measured by summing the 3,000 $cm^3$ vented during the experiment to the gas released at the end of the experiment, when the cell was depressurized to 3.5 MPa. The fact that so little gas had to be vented in order to keep the system pressure below 21 MPa suggests that the cell pressure would not have significantly exceeded this maximum pressure had the gas not been released. Both results for pressure buildup are within the experimental error of predictions made by the Peng-Robinson equation of state.

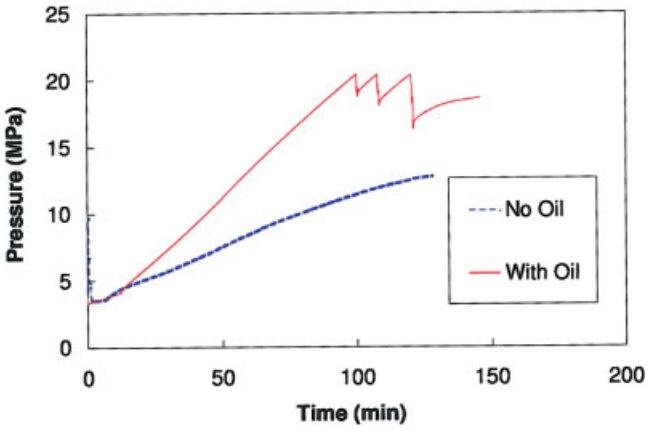


**Figure 11. Pressure transducer readings during dissociation of a hydrate plug in a sealed system.**

[Color figure can be viewed in the online issue, which is available at www.interscience.wiley.com.]

Uneven heat input was also investigated to simulate partial failure of an electrical heating system. The experiments were conducted on structure I hydrate plugs. The heat flux was applied to half of the cell on which the pressure safety valve (PSV) was installed, and gas released from the valve at other side to maintain the cell pressure. Power inputs of 15 and 30 W were investigated.

Figure 12 compares the dissociation rate of a hydrate plug subjected to 30 W of heat applied to the radial surface of one half of the plug to the dissociation rate of a plug where the heat was applied evenly over the whole length. The dissociation rate is significantly decreased by the additional heat-transfer resistance between the heated half of the plug and the remaining hydrate at the opposite end of the plug, as shown in Figure 12.

## Conclusions

The dissociation rate of an industrial hydrate plug is predicted using a one-dimensional (1-D) heat-transfer model in cylindrical coordinates. The model can predict the total dissociation time by two-sided depressurization, and by evenly applied radial heat input to within 10% with no fitted parameters, provided sufficient knowledge of the properties of the plug are available.

The experimental results confirmed that hydrate dissociation in the systems investigated were heat-transfer limited; mass transfer, intrinsic and dissolution kinetics appear to be

sufficiently fast that they do not limit the dissociation rate. It is possible that kinetics becomes important under high-heat fluxes.[35]

The experiments confirm that for hydrate plugs with a diameter substantially less than the axial length then the hydrate will dissociate radially if depressurized from both ends.

The model predicts that sII will dissociate more slowly than sI owing to its higher latent heat. This was repeatedly demonstrated experimentally.

The assumption that the temperature of the hydrate phase is not a function of radius appears to be valid for the laboratory experiments where the hydrate temperature remains constant for the duration of the experiment. This assumption is likely to be less valid for systems where the pressure accumulates rapidly, thus, raising the dissociation temperature.

The model predictions are sensitive to the plug porosity, and in the case of the one-sided model to plug permeability. In industrial applications, these properties are rarely known. This limits the application of the models to an order of magnitude prediction of the dissociation time. The models can be used to perform a sensitivity analysis on these parameters in order to determine the best and worst case dissociation times before dissociating a plug.

The properties of the plug are likely to depend greatly on the formation conditions. Ongoing attempts to model the multiphase flow in oil and gas transmission lines may eventually yield a better understanding of how plugs form and allow engineers to better predict these properties more accurately.

The model can also be used to predict the plug radius as a function of time, which could be applied to determine when the annulus spacing is large enough to introduce a thermodynamic hydrate inhibitor, such as methanol, to expedite the plug dissociation.

The one-sided dissociation model is the most computationally intensive component and has had limited experimental validation owing to problems creating a laboratory scale plug with a low permeability. The model overpredicts the dissociation time for laboratory scale hydrates, and underpredicts it for industrial hydrates.

The electrical heating model can be combined with considerations of the flow rate of the gas released through the annulus formed around the plug, to calculate the maximum allowable rate of heat input to avoid localized overpressurization of the flowline.

The models presented in this article have been successfully applied to simulate the dissociation of industrial hydrate plugs,[36] and have proven to be useful tools when deciding on an effective remediation strategy.

## Acknowledgments

The authors wish to acknowledge the financial support received from the DeepStar consortium of energy companies. Thanks are also due T. Hughes for his help with experimental measurements, and K. C. Hester for Raman spectroscopy measurements.

## Notation

$A_p$ = surface area of hydrate particle, $m^2$
$B_i$ = Biot number
$C_{pH}$ = water specific heat capacity, $Jkg^{-1}K^{-1}$
$C_{pW}$ = hydrate specific heat capacity, $Jkg^{-1}K^{-1}$
$k_w$ = thermal conductivity of water, $Jm^{-1}s^{-1}K^{-1}$
$k_{wall}$ = thermal conductivity of wall, $Jm^{-1}s^{-1}K^{-1}$
$L_c$ = length of hydrate plug, m
$m_H$ = mass of hydrate remaining, kg
$m_w$ = mass of free water, kg
$P_d$ = downstream pressure, $Nm^{-2}$
$P_u$ = upstream pressure, $Nm^{-2}$
$Q_H$ = rate of heat transfer to hydrate plug, $Js^{-1}$
$Q_{IN}$ = rate of heat transfer to cell contents, $Js^{-1}$
$r$ = radial position, m
$r_0$ = flowline radius, m
$r_H$ = radial position of hydrate front, m
$r_I$ = radial position of ice front, m
$T_0$ = ambient temperature, K
$T_d$ = downstream temperature, K
$T_D$ = hydrate dissociation temperature, K
$T_H$ = hydrate plug temperature, K
$T_I$ = ice layer temperature, K
$T_u$ = upstream temperature, K
$T_W$ = water temperature, K
$t$ = time, s
$z$ = axial distance, m

### *Greek letters*

$\alpha_w$ = thermal diffusivity of water, $m^2s^{-1}$
$\beta$ = volume expansivity, $K^{-1}$
$\varepsilon$ = porosity of hydrate plug, $m^3m^{-3}$
$\kappa$ = permeability, $kgPa^{-1}s^{-1}m^{-2}$
$\lambda$ = stability criterion
$\lambda_H$ = enthalpy change of dissociation, $Jkg^{-1}$
$\lambda_I$ = latent heat of ice melting, $Jkg^{-1}$
$\mu$ = fluid viscosity, $Nm^{-2}s$
$\xi$ = mass of water per mass of methane hydrate
$\pi$ = pi
$\rho_H$ = density of hydrate, $kgm^{-3}$
$\rho_I$ = density of ice, $kgm^{-3}$

## Literature Cited

1. Sloan ED. *Clathrate Hydrates of Natural Gasses*. 2nd ed., New York, Marcel Dekker; 1998.
2. Priestly J. *Experiments and Observations on Different Kinds of Air and Other Branches of Natural Philosophy Connected with the Subject*. In Vol. 3, T. Pearson; 1790.
3. Hammerschmidt EG. Formation of gas hydrates in natural gas transmission lines. *Ind. Eng. Chem.* 1934;26:851.
4. Milkov AV. Global estimates of hydrate-bound gas in marine sediments: How much is really out there? *Earth-Sci. Reviews*. 2004;66: 183–197.
5. Kelkar SK, Selim MS, Sloan ED. Hydrate dissociation rates in flowlines. *Fluid Phase Equilibria*. 1998;371:150–151.
6. Kofoed EE, Østergaard KK, Tohedi B. A Quasi Steady-State Model for the Dissociation of Gas Hydrates in Flowlines. *4th International Conference on Gas Hydrates*. Yokahama, Japan; 2002;304–313.
7. Lysne D. *An Experimental Study of Hydrate Plug Dissociation by Pressure Reduction*. University of Trondheim, 1995. PhD Thesis.
8. Peters DJ. *A Study of Hydrate Dissociation in Flowlines by the Method of Two-Sided Depressurization: Experiment and Model*. Colorado School of Mines; 1999. Masters Thesis.
9. Bollavaram P. *Hydrate Plug Dissociation in Flowlines by Pressure Reduction: Experiment and Modeling*. Colorado School of Mines; 2002. PhD Thesis.
10. Davies SR, Ivanic J, Sloan ED. Predictions of Hydrate Plug Dissociation with Electrical Heating. *Proc. 5th International Conference on Gas Hydrates*. Trondheim; 2005;4:1396–1405.
11. Sloan ED. *Hydrate Engineering*. 1st ed. SPE Monograph Vol. 21. Henry L. Doherty Series; 2000.
12. Cochran S. Hydrate-Control and Remediation Best Practices in Deepwater Oil Developments. *Offshore Technology Conference*, OTC 15255. Houston, TX; 2003.

13. Løken KP, Li X, Austvik T. The Hydrate Control Strategy for the Åsgard Field and Hydrate Plug Melting using the Bundle Heating Method. *Multiphase Technology Conference*. Cannes; 1999.
14. Urdahl O, Børnes AH, Kinnari KJ, Holme R. Operational Experience by Applying Direct Electrical Heating for Hydrate Prevention. *Offshore Technology Conference*. Houston, TX; 2003.
15. Mehta A, Hudson J, Peters DJ. Risk of Flowline Over-Pressurization during Hydrate Remediation by Electrical Heating. *Deepwater Flowline and Riser Technology Conference*. Houston, TX; 2001.
16. Stern LA, Kirby SH, Durham WB. Peculiarities of methane clathrate hydrate formation and solid-state deformation, including possible superheating of water ice. *Science*. 1996;273(5283):1843–1848.
17. Hwang MJ, Wright DA, Kapur A, Holder GD. An experimental study of crystallisation and crystal growth of methane hydrates from melting ice. *J of Inclusion Phenomena and Molecular Recognition in Chem*. 1990;8:103–116.
18. Henning RW, Schultz AJ, Thieu V, Halpern Y. Neutron diffraction studies of $CO_2$ clathrate hydrate: Formation from deuterated ice. *J of Phys Chem*. 2000;104;5066–5071.
19. Peng D, Robinson DB. Two and three phase equilibrium calculations for systems containing water. *Can J of Chem Eng*. 1976;54:595–599.
20. Ballard AL, Sloan ED, Jr. The next generation of hydrate prediction I. Hydrate standard states and incorporation of spectroscopy. *Fluid Phase Equilibria*. 2002;194–197:371–383.
21. Subramanian S, Sloan ED. Trends in vibrational frequencies of guests trapped in clathrate hydrate cages. *J of Phys Chem B*. 2002; 106:4348–4355.
22. De Boer RB, Houbolt JJHC, Lagrand J. Formation of gas hydrates in a permeable medium. *Geologie en Mijnbouw*. 1985;64:245–249.
23. Bird RB, Stewart WE, Lightfoot EN. *Transport Phenomena*. 2nd ed. Wiley; 2002.
24. Incropera FP, DeWitt DP. *Fundamentals of Heat and Mass Transfer*. 4th ed. Wiley; 1996.
25. Morrison FA. Transient gas flow in a porous column. *Ind and Eng Chem Fundamentals*. 1972;11(2):191.
26. Pozrikidis C. *Numerical Computation in Science and Engineering*. Oxford University Press; 1998.
27. Leonard BP. A Stable and Accurate Convective Modeling Procedure Based on Quadratic Upstream Interpolation. *Comp Methods in Appl Mech and Eng*. 1979;19:59–98.
28. Hoffman JD. *Numerical Methods for Engineers and Scientists*. New York: Marcel Dekker; 2001.
29. Gupta A, Sloan ED, Kneafsey TJ, Tomutsa L, Moridis G. Modeling Methane Hydrate Dissociation X-ray Computer Tomography Data Using a Heat Transfer Model. *Proc. 5th International Conference on Gas Hydrates*. Trondheim; 2005;2:2004.
30. NIST Chemistry WebBook, NIST Standard Reference Database Number 69, June 2005 Release. Available online at: http://webbook.nist.gov/chemistry/
31. Ivanic J. *Hydrate Plug Dissociation: Investigations of Two-Sided Depressurization*. Colorado School of Mines; 2004. Masters Thesis.
32. Huang D, Fan S. Measuring and Modeling Thermal Conductivity of Gas Hydrate-Bearing Sand. *J of Geophysical Res*. 2005;110:B01311.
33. Berge L, Gjertsen L, Lysne D. The Importance of Porosity and Permeability for Dissociation of Hydrate Plugs in Pipes. Proc. *2nd International Conference on Gas Hydrates*. Toulouse, France; 1996: 533–540.
34. Berge L, Gjertsen L, Lysne D. Measured Permeability and Porosity of R11 ($CCl_3F$) Hydrate Plugs. *Chem Eng Sci*. 1998;53(9):1631–1638.
35. Jamaluddin AKM, Kalogerakis N, Bishnoi PR. Modelling of Decomposition of a Synthetic Core of Methane Gas Hydrate by Coupling Intrinsic Kinetics with Heat Transfer Rates. *The Can J of Chem Eng*. 1989;67:948–954.
36. Kashou S, Subramanian S, Matthews P, Thummel L, Faucheaux E, Subik D, Qualls D, Akey R, Carter J. GOM Export Gas Flowline, Hydrate Detection and Removal. *Offshore Technology Conference* OTC 16691. Houston, TX; 2004.

*Manuscript received May 25, 2006, and revision received July 10, 2006.*